

Ultrasonic welding of magnetic hybrid material systems –316L stainless steel to Ni/Cu/Ni-coated Nd₂Fe₁₄B magnets

Moritz Liesegang (✉ liesega@mv.uni-kl.de)

TU Kaiserslautern: Technische Universität Kaiserslautern <https://orcid.org/0000-0003-3062-794X>

Tilmann Beck

TU Kaiserslautern: Technische Universität Kaiserslautern

Research

Keywords: Ultrasonic welding, functional hybrid material systems, rare earth permanent magnets, hybrid joints

Posted Date: January 28th, 2021

DOI: <https://doi.org/10.21203/rs.3.rs-88532/v2>

License: © ⓘ This work is licensed under a Creative Commons Attribution 4.0 International License.

[Read Full License](#)

Version of Record: A version of this preprint was published at Functional Composite Materials on March 22nd, 2021. See the published version at <https://doi.org/10.1186/s42252-021-00017-1>.

Abstract

The performance of electric sensors is continuously improving due to the demands of modern vehicles and electronic devices. Magnetic sensors are used in a wide field of applications. However, handling and mounting the typical high-performance rare earth permanent magnets are challenging due to their brittleness. A constant magnetic flux is a key property of the magnetic setup in many devices. State-of-the-art adhesive bonding of magnets in devices can cause problems due to the low durability and viscous behaviour of adhesive polymers, as the magnet may change its position and hence, the magnetic flux distribution in the magnetic setup changes.

Ultrasonic welding is a powerful technique to join hybrid material systems quickly and reliably, providing high joint strength, even for brittle materials such as glasses, ceramics and rare earth permanent magnets. The latter is being investigated in this work for the first time. The ultrasonic welding process was adapted to join 316L stainless steel, representing potential components of magnetic devices, to Ni/Cu/Ni-coated $\text{Nd}_2\text{Fe}_{14}\text{B}$. In addition to directly joined steel/magnet-hybrids, ductile aluminium and nickel interlayers were used in order to enhance the joint strength.

Process parameters were developed and evaluated considering the resulting shear strength of the joints. The highest shear strength of 35 MPa was achieved for 316L/ $\text{Nd}_2\text{Fe}_{14}\text{B}$ and 316L/Al/ $\text{Nd}_2\text{Fe}_{14}\text{B}$, which is more than twice the shear strength of adhesively bonded joints of up to 20 MPa, according to the literature. The functional performance of the hybrid material systems, evaluated by the magnetic flux density of the hybrid material systems was the highest for directly bonded joints, and those with a nickel interlayer, which did not show any losses in comparison to the single magnet in its initial state. Joints with an aluminium interlayer showed losses of 3% and adhesively bonded joints showed losses of 7% of the magnetic flux density.

In summary, the results of this work indicate that ultrasonic welding is a suitable technique to improve the production process and performance of magnetic devices.

1. Introduction

Permanent magnets are used in electric motors, generators or actuators, as well as in diverse magnetic sensors, their chief purpose being to provide a constant magnetic flux [1,2]. Ferromagnetic steels, ceramic hard magnetic ferrites as well as alloys such as AlNiCo or sintered SmCo and NdFeB are potential materials for magnetic devices [2]. The strength of the magnetic field the magnets can create, the magnetization M , and the resistance against opposing magnetic fields, the coercive field H_c determine the performance of permanent magnets, typically measured by the maximum energy density product $(BH)_{\max}$ [3]. Rare earth permanent magnets such as SmCo or NdFeB are the most performant commercial permanent magnets. NdFeB type magnets provide the highest magnetization and SmCo type magnets can tolerate high temperature applications up to 350°C and have higher coercive fields as well as corrosion resistance [4–6].

The time stability of the magnetic flux is a fundamental requirement, especially for magnetic sensors, to assure reliable measurements as small changes of intrinsic magnetic properties or the position of the magnet in the measurement setup affect the accuracy of the sensors [7–9].

Due to the brittleness of rare earth permanent magnets, handling and mounting are challenging [10]. Permanent magnets are typically mounted by adhesives, such as epoxy resins, and rarely by mechanical interlocking into diverse magnetic sensor devices [10–13]. The strength and durability of adhesive bonds are relatively low compared to other joining methods and, most importantly, the mechanical properties of the joints change during the lifetime of the device because of the viscosity of polymers [10,14,15].

Using adhesive joining techniques, applications at temperatures higher than 150°C are also problematic as the joint strength decreases at elevated temperatures despite the use of high-performance polymers, such as Polyphenylene sulphide (PPS) [16].

Ultrasonic welding is one promising technique to realise hybrid joints between metallic substrates and brittle permanent magnets. So far, ultrasonic welding is mostly used in the packaging industry to reliably join polymers quickly and cost-effectively [17], or to join soft non-ferrous metals such as aluminium and copper for electrical applications [18]. Ultrasonic welding of hybrid material systems, such as metal/CFRP joints, has been a focus of research during the last decade. For example, aluminium/CFRP joints have been investigated [19–22]. In addition several multi-metal combinations like aluminium and magnesium, copper, steel or titanium have been ultrasonically welded [23–28].

Ultrasonic welding of brittle materials, such as glasses and ceramics with metals is challenging and has been investigated, partially using an air beared anvil and a ductile aluminium interlayer to ensure homogeneous stress distribution on the joining partners and to prevent damage to the brittle glass and ceramic parts [29,30].

According to literature the success of the ultrasonic welding process depends on process and material parameters. Welding amplitude, force and energy, or time are important process parameters, while mechanical properties, geometry and surface topography are material and geometrical parameters, respectively, that affect the joining quality [20].

The process parameters interact with each other and hence, always have to be assessed in combination.

The sonotrode oscillates with a certain amplitude, inducing an equivalent elastic and plastic deformation amplitude in the joining partners, that are closely pressed together by the welding force. The welding energy is typically defined as the product of the generator power and the welding time. A suitable amplitude has to be chosen in order to allow an adequate deformation without damaging the joining partners. A sufficiently high welding force is essential for a close contact of the joining partners in the interface without inhibiting the oscillation or damaging the joining partners. The welding energy is the time dependent power provided by the ultrasound generator which hence, is suitable control parameter for the ultrasonic welding machine. In comparison to simply control the process by welding time, the

welding energy includes the amplitude and the welding force that directly influence the generator power [31–33].

Regardless of the ultrasonic welding type (i.e. polymer or metal ultrasonic welding subdivided in spot-, torsional, or seam welding), a sufficient amount of energy has to be induced into the joining zone by oscillation in contact with the upper joining partner since the formation of joints by ultrasonic welding is caused by the relative motion between the joining partners. In the case of metal/metal joints, as investigated in this work, the peaks of the topography are flattened and plastically deformed and the surface structures of the joining partners assimilate in the first step. Afterwards, oxide layers on the surfaces are locally broken up, which allows a direct metal/metal contact between the joining partners additional to mechanical interlocking. [23,25,34–37]

The aim of the presented investigations is the formation of high performance 316L/Nd₂Fe₁₄B joints for the first time to compete state-of-the-art adhesive joining featuring high joint strength as well as a speedy and reliable joining process. Hence, 316L flat rings, representing potential components of magnetic devices, are welded to thermally demagnetized Nd₂Fe₁₄B, one of the most common rare earth permanent magnetic materials [4–6], with the typical ~25 µm thick Ni/Cu/Ni coating against corrosion [38,39].

To quantify the performance of the hybrid material systems, the joint strength and the magnetic flux density were determined and evaluated in relation to the flux of a single Nd₂Fe₁₄B, magnet in its initial state.

2. Materials And Experimental

The aim of the presented investigations was to develop high strength 316L/Nd₂Fe₁₄B joints. Figure 2 shows the sample geometry and microstructure of 316L stainless steel and Nd₂Fe₁₄B samples including the ~25 µm thick Ni/Cu/Ni coating applied to the latter. The 316L microstructure revealed an average grain size of 22 µm with a relatively homogeneous distribution. The microstructure of Nd₂Fe₁₄B is typical for sintered NdFeB type magnets. The average grain size of 5 µm was homogeneous, whereas the porosity, ~4% in average, increases towards the surface or the coating.

As mentioned in the introduction, the main aim was to effect a direct connection between the coated Nd₂Fe₁₄B magnet and the 316L stainless steel in order to avoid any additional material, such as adhesives or interlayers reducing the magnetic flux and, therefore, the performance of the components. Nevertheless, besides directly joining steel and magnets, aluminium (thickness 0.1 mm), nickel (thickness 0.2 mm) foils and epoxy resin were used to compare the joint's strength.

As outlined above, the joint was partially formed by plastic deformation of the surfaces of the joining partners, which depended on the mechanical properties of the joining partners and the topography of their contact surface. Relevant properties are listed in Table 1. Because this research may be relevant to other rare earth permanent magnetic materials, Sm₂Co₁₇ is listed for comparison. Sm₂Co₁₇'s mechanical

properties are relatively similar to $\text{Nd}_2\text{Fe}_{14}\text{B}$'s and, therefore, the ultrasonic weldability is expected to be comparable. Considering the interlayers in comparison to the surrounding joining partners, low Young's moduli, yield strengths and hardnesses are preferable, while ductility, represented by the elongation to fracture should be high, as the interlayer is supposed to deform plastically during the welding process, operating as a coupling agent. Note that, in comparison with both considered interlayers, the strength and hardness of $\text{Nd}_2\text{Fe}_{14}\text{B}$ was significantly higher. The topography of the contact surface affects the interaction of the joining partners at the interface during the welding process [33]. Even though the impact of different surface topographies was not investigated in this work, the surface roughness of all joining partners is listed in Table 1 for documentation purposes.

Table 1: Mechanical properties and surface roughness of the materials used in the welding experiments

	Young's modulus in GPa	Yield strength in MPa	Hardness HV10	Elongation to fracture in %	Surface roughness R_a in μm
	[40]	[40]	[40]		
$\text{Nd}_2\text{Fe}_{14}\text{B}$	152-157	250-285	550	4% [41]	-
Ni/Cu/Ni	-	-	170	-	0.34 ± 0.08
$\text{Sm}_2\text{Co}_{17}$	117	110	500	-	-
316L	200	310	170	30% [40]	0.74 ± 0.05
AA 1050	70	48	20	45% [40]	0.32 ± 0.01
Ni 2.4068	190-220	90	170	40% [40]	0.26 ± 0.01

All welded joints were realised by ultrasonic welding using a 20 kHz Telsonic TSP 9000 torsional welding machine and a sonotrode with a maximum amplitude of 22 μm of the mechanical oscillation at the outer diameter of the sonotrode tip. The setup of the welding machine is shown in Figure 3. The oscillation was induced by four piezoelectric transducers providing a maximum power of 10 kW transducing the high frequency electric voltage into the mechanical oscillation. The longitudinal oscillation was then induced into the four boosters that drive the torsional oscillation of another booster and, finally, of the sonotrode itself. The welding energy was induced by the oscillating sonotrode tip, superimposed by the welding force of up to 5 kN applied in vertical direction along the torsional oscillation unit by a pneumatic cylinder.

As mentioned before, ultrasonic welding of brittle materials is challenging because the materials are prone to damage as a result of stress concentrations combined with the vibration applied during the welding process. To prevent stress peaks on the surface that are caused by non-parallelism of the joining

partners and the sonotrode tip, an air beared anvil was used, which is shown in Figure 4. Compressed air streams around the sample holder adjusting its tilt in relation to the sonotrode tip when a force is applied. The samples were placed in a groove in the centre of the sample holder to ensure that the welding samples and sonotrode tip were well centred. After cleaning with ethanol, all hybrid material systems were joined with the 316L flat rings as upper and the NdFeB type magnets as lower joining partner.

Suitable process parameters determine the feasibility of joining at all and have a significant impact on the joint quality. The amplitude of the sonotrode oscillation, the welding energy and the welding pressure or welding force are the key process parameters that need to be adjusted dependent on the joining partners. The profile of the sonotrode tip is typically another important parameter, but is not in the focus of this work. The sonotrode used in this work had a fine pyramidal structure.

The determination of process parameters is challenging as both, the amplitude and the welding pressure affect the welding energy. In order to obtain a high joint strength, welding parameters were investigated by a design of experiments (DoE) approach using the software Umetrics MODDE 7 to plan 24 process parameter setups with 4 repetitions for each setup in 2 blocks, i.e. 96 welding experiments in total. In this model the amplitude, the welding energy and the welding force are the factors to be varied in order to achieve a certain shear strength as response. The investigated parameter setups are determined by a randomized "center composite circumscribed" model (CCC) varying the amplitude from 12 to 15 μm , i.e. 50-60% of the joining device's capability, the welding energy from 40 to 250 J and the welding pressure from 0.05 to 2 bar, corresponding to welding forces between 80 and 1500 N, based on extensive preliminary experiments.

Note that the welding amplitude was tuned by the power the generator provided to the piezoelectric transducer and hence is indicated in both, % and μm . Furthermore, the welding force was tuned by air pressure attached to a pneumatic cylinder and therefore is indicated in both, bar and N. The relation between welding force and air pressure was determined by an independent force sensor.

For all parameter sets the welding time was below 1 second, showing the outstanding process speed, especially in comparison to adhesive joining techniques [42].

The process parameters were evaluated by the resulting joint strength, determined by shear tests. The shear tests were performed with a 25 kN Schenk tensile testing machine, using a shear testing insert, which is illustrated in Figure 5. The joints are placed in a groove and sheared by the relative motion of the upper and the lower part of the insert, driven by the tensile testing machine with a crosshead speed of 3 mm/min. To compare the shear strength of ultrasonically welded joints with and without ductile Ni- and Al-interlayers to state-of-the-art adhesive joining, epoxy resin was used to join six additional samples.

Measurements of the open circuit magnetic flux density were performed by a hall sensor to determine the influence of the setup of the hybrid joints on the magnetic performance. The different thicknesses of the joints were considered and balanced by a constant distance of 50 mm between the surface of the magnet and the sensor. The loss of magnetic flux density of the hybrid material systems was determined

in comparison to a single $\text{Nd}_2\text{Fe}_{14}\text{B}$ magnet in its initial state. The setup of the magnetic measurements is shown schematically in Figure 6 for a directly welded 316L/ $\text{Nd}_2\text{Fe}_{14}\text{B}$ as example.

3. Results And Discussion

The influence of the parameter setups was investigated by DoE. The process parameters amplitude, welding pressure and welding energy were combined in order to maximize the resulting shear strength. The relation between the process parameters investigated and the resulting shear strength calculated by multiple linear regression of the experimental results, is illustrated by the surface plots in Figure 7. The calculated maximum shear force is shown depending on the combination of a) welding energy and pressure at an amplitude of 56%/14 μm and of b) amplitude and welding energy at a welding pressure of 1.55 bar.

The surface plots show explicit maxima, which allow to identify the most promising process parameters. An amplitude of 14 μm (56%), a welding force of 1000 N (1.25 bar), and a welding energy of 140 J were determined to obtain a predicted maximum shear force of 142 N, according to the surface plots in Figure 7. Six samples were welded to verify the determined parameters achieving a maximum shear force of 177 N \pm 12 (7% mean absolute deviation), which is even higher than predicted. The multiple linear regression for the prediction includes the inaccuracy of the welding experiments, which explains the gap between predicted and actual joint strength. One big advantage of ultrasonic welding is the process security and reproducibility of welding qualities, if sample holders and samples are suitable. However, a deviation of 7% is acceptable, considering differences e.g. in the surface quality of the joining partners or the adhesive strength between the Ni/Cu/Ni coating and NdFeB type magnet. Based on the process parameters determined by the DoE, joints with aluminium and nickel interface were also ultrasonically welded. The direct transfer of ultrasonic welding parameters to other hybrid material systems is hardly possible. Nevertheless, suitable welding parameters were determined in approximately 20 welding experiments, following the parameters determined by DoE for 316L/NdFeB.

Table 2: Process parameter sets for the ultrasonically welded hybrid material systems investigated

	amplitude in % / μm	welding pressure in bar / N	welding energy in J
316L/ $\text{Nd}_2\text{Fe}_{14}\text{B}$	56 / 14	1.25 / 1000	140
316L/Al99/ $\text{Nd}_2\text{Fe}_{14}\text{B}$	50 / 12	1.5 / 1250	200
316L/Ni/ $\text{Nd}_2\text{Fe}_{14}\text{B}$	50 / 12	2 / 1600	100

An example of every ultrasonically welded hybrid material system (a), investigated in this work and the respective fracture surfaces of the joining partners after the shear test (b, c) is shown in Figure 8. Despite a slight sonotrode imprint, the 316L flat ring, the $\text{Nd}_2\text{Fe}_{14}\text{B}$ round plate and the Ni/Cu/Ni coating as well as the nickel foil do not appear to have been affected by the welding process. However, the aluminium foil warped up during welding. All samples failed at the 316L stainless steel interface with its joining partner.

The width of the fracture surfaces indicating the effective joint areas of the different hybrid material systems revealed big differences due to the differences of the ductility of the joining partners. Therefore, the achieved maximum shear forces could not be compared between different hybrid material systems. Hence, the joint areas of six samples of each joint tape were measured by the contrast difference obtained using the software imagic IMS to determine the shear strength in MPa. The determined joint properties of all hybrid material systems investigated in this work are listed in Table 3.

Table 3: Determined joint properties of all hybrid material systems investigated

	maximum shear force in N	joint area in mm^2	shear strength in MPa
316L/ $\text{Nd}_2\text{Fe}_{14}\text{B}$	177 ± 12	5 ± 1	35 ± 6
316L/Al99/ $\text{Nd}_2\text{Fe}_{14}\text{B}$	1100 ± 111	31 ± 0	35 ± 3
316L/Ni/ $\text{Nd}_2\text{Fe}_{14}\text{B}$	216 ± 4	8 ± 0.5	27 ± 3
316L/epoxy/ $\text{Nd}_2\text{Fe}_{14}\text{B}$	120 ± 36	62 ± 0	2 ± 2.5

The preparation of the surfaces is a key aspect to achieve good joint strength of adhesively joined connections and may have caused the significantly lower joint strength of the adhesively joined samples prepared in this work. Hence, the shear strength of similar hybrid material systems of up to 22 MPa [43,44] was compared to ultrasonically welded samples, revealing a significantly higher joint strength for all ultrasonically welded samples in this work. Despite the promising results of achieving high joint shear stress by direct welding of 316L to $\text{Nd}_2\text{Fe}_{14}\text{B}$ using the process parameters obtained by DoE, it has to be considered that the joint contact area was smaller compared to the contact zone of samples with nickel and especially, with aluminium interlayer.

The microstructure of the joints is shown in Figure 9. Only joints with an aluminium interlayer (316L/Al-foil/ $\text{Nd}_2\text{Fe}_{14}\text{B}$) showed a full-surface bonding. At the microscale the directly bonded joints and those with a nickel interlayer were connected only partially, relevant to the fracture surfaces observed. However, in the case of directly bonded joints, the connection between 316L and the Ni/Cu/Ni coating was very close because the surfaces were assimilated and mechanically locked. Apparently, the plastic deformation of

the Ni/Cu/Ni was so large that even the inner copper layer was deformed. In the case of joints with an interlayer, only the outer Ni layer of the Ni/Cu/Ni-coating was plastically deformed to assimilate with the surface of the other joining partner.

In the case of joints with an aluminium interlayer, the aluminium foil did assimilate with the Ni/Cu/Ni coating but significantly less so with the surface of 316L in comparison to the directly welded samples. The nickel interlayer assimilated even less. In addition to the fact that the connection only occurred partially, the nickel foil assimilated less with both the 316L and the Ni/Cu/Ni surfaces.

The fracture surfaces in Figure 8 show the failure of the hybrid material systems between the 316L flat rings and the joining partners. To further analyse the failure behaviour, all fracture surfaces were investigated by scanning electron microscopy (SEM) and energy dispersive X-Ray (EDX) analysis. All fracture surfaces included remaining material adherence of the opposite joining partner, which was identified by EDX. This means, that the joints did not solely fail in the interlayer between the joining partners, but rather in the volume of the joining partners with lower shear strength. An example is shown for a 316L/NdFeB joint in Figure 10, showing the fracture surface of 316L with remaining nickel clusters from the Ni/Cu/Ni coating of the magnet on the 316L flat ring. The related secondary electron (SE) image (Figure 10 a) shows the 316L surface. The arrows indicate one of the nickel clusters that remained after shear testing the ultrasonically welded hybrid material systems as example, confirmed by the higher nickel and the lower iron concentration in the certain area, measured by EDX. Partially, the joints even failed in the volume of the magnet, shown in the microsection of a failed joint in Figure 10 d). The numerous nickel clusters that remained on the 316L flat ring after shear test and the failure in the Nd₂Fe₁₄B volume explain the high joint strength caused by a connection on a microstructural level.

Finally, the magnetic performance is as important as the joint quality to ensure the functionality of the hybrid joints. The magnetic flux density, shown in Table 4, was 3% lower for samples with an aluminium interlayer and 7% lower for adhesively bonded joints in comparison to samples with a nickel interlayer, as well as the directly welded samples, which did not show any change of magnetic flux density because of the setup of the hybrid material system.

Table 4: Loss of magnetic flux density of the hybrid material systems in relation to a single Nd₂Fe₁₄B magnet in its initial state

	loss of magnetic flux density in %
316L/Nd ₂ Fe ₁₄ B	0 ± 5·10 ⁻³
316L/Al99/Nd ₂ Fe ₁₄ B	3 ± 5·10 ⁻³
316L/Ni/Nd ₂ Fe ₁₄ B	0 ± 5·10 ⁻³
316L/epoxy/Nd ₂ Fe ₁₄ B	7 ± 2

4. Summary

Hybrid joints of 316L stainless steel and $\text{Nd}_2\text{Fe}_{14}\text{B}$ rare earth permanent magnets were successfully realised by torsional ultrasonic welding. Three different joint material systems were investigated. Directly joined 316L stainless steel to Ni/Cu/Ni-coated demagnetized $\text{Nd}_2\text{Fe}_{14}\text{B}$ (316L/ $\text{Nd}_2\text{Fe}_{14}\text{B}$), and joints of the same materials with additional ductile aluminium and nickel interlayers (316L/Al/ $\text{Nd}_2\text{Fe}_{14}\text{B}$ and 316L/Ni/ $\text{Nd}_2\text{Fe}_{14}\text{B}$) were realised. A promising shear strength of 35 MPa for 316L/ $\text{Nd}_2\text{Fe}_{14}\text{B}$ and 316L/Al/ $\text{Nd}_2\text{Fe}_{14}\text{B}$ was achieved as well as 27 MPa for 316L/Ni/ $\text{Nd}_2\text{Fe}_{14}\text{B}$, which are significantly higher in comparison to adhesively bonded joints. An observation of the microstructure revealed a direct contact between the joining partners, despite the less pronounced assimilation and interlocking of the surfaces in case of joints with aluminium and nickel interlayers. The magnetic performance, evaluated by magnetic flux density of magnetized $\text{Nd}_2\text{Fe}_{14}\text{B}$, showed a slightly lower performance for 316L/Al/ $\text{Nd}_2\text{Fe}_{14}\text{B}$ joints caused by the aluminium layer in the setup of the hybrid material system.

Despite the potential enhancement of the joint quality of the hybrid material systems investigated in respect of the joint area, the results of this work indicate that ultrasonic welding is a promising technique in order to enhance the production process and the performance of magnetic devices. Prospective investigations may include the influence of surface conditions of the joining partners, layer and interlayer thickness as well as the detailed analysis of the process parameters over the welding time.

5. Declarations

Availability of data and materials

The datasets used and analysed during the current study are available from the corresponding author on reasonable request.

Competing interests

The authors declare no competing financial interests.

Funding

This research received no specific grant from any funding agency in the public, commercial, or not-for-profit sectors.

Authors' contributions

ML developed the process parameters for the ultrasonic welding experiments, analysed the joint quality, obtained the corresponding magnetic data and was the major contributor in writing the manuscript. ML and TB extensively discussed the results, as well as read and approved the manuscript.

Acknowledgement

We thank our colleagues Benjamin Beck and Lars Greipl for their assistance on the welding experiments and the shear testing of the welded samples. Gratitude is also expressed to Anna Julia Raupach and Wolfgang Guth for their patience during the challenging preparation of the microsections. Sincere thanks also go Dr. Matasha Mazis for proofreading.

References

- [1] J.M.D. Coey, Permanent magnet applications, *Journal of Magnetism and Magnetic Materials* 248 (2002) 441–456. [https://doi.org/10.1016/S0304-8853\(02\)00335-9](https://doi.org/10.1016/S0304-8853(02)00335-9).
- [2] O. Gutfleisch, M.A. Willard, E. Brück, C.H. Chen, S.G. Sankar, J.P. Liu, Magnetic materials and devices for the 21st century: stronger, lighter, and more energy efficient, *Advanced materials* (Deerfield Beach, Fla.) 23 (2011) 821–842. <https://doi.org/10.1002/adma.201002180>.
- [3] J. Fischbacher, A. Kovacs, M. Gusenbauer, H. Oezelt, L. Exl, S. Bance, T. Schrefl, Micromagnetics of rare-earth efficient permanent magnets, *Journal of Physics D: Applied Physics* 51 (2018) 193002. <https://doi.org/10.1088/1361-6463/aab7d1>.
- [4] O. Gutfleisch, Controlling the properties of high energy density permanent magnetic materials by different processing routes, *Journal of Physics D: Applied Physics* 33 (2000) R157-R172. <https://doi.org/10.1088/0022-3727/33/17/201>.
- [5] M. Duerrschnabel, M. Yi, K. Uestuener, M. Liesegang, M. Katter, H.-J. Kleebe, B. Xu, O. Gutfleisch, L. Molina-Luna, Atomic structure and domain wall pinning in samarium-cobalt-based permanent magnets, *Nature communications* 8 (2017) 54. <https://doi.org/10.1038/s41467-017-00059-9>.
- [6] W. Rodewald, B. Wall, M. Katter, K. Uestuener, Top Nd-Fe-B magnets with greater than 56 MGOe energy density and 9.8 kOe coercivity, *IEEE Trans. Magn.* 38 (2002) 2955–2957. <https://doi.org/10.1109/TMAG.2002.803075>.
- [7] M. Liesegang, R. Regnat, K. Uestuener, F.-J. Boergermann, M. Katter, Influence of the Sample Position on the Measured Magnetic Flux in Helmholtz Coils Biased with Halbach Array Systems, *International Workshop on Rare-Earth and Future Permanent Magnets and their Applications*, Darmstadt, 2016.
- [8] M. Haavisto, S. Tuominen, T. Santa-Nokki, H. Kankaanpää, M. Paju, P. Ruuskanen, Magnetic Behavior of Sintered NdFeB Magnets on a Long-Term Timescale. *Advances in Materials Science and Engineering*, 2014, 1-7 (2014). <https://doi.org/10.1155/2014/760584>.
- [9] R.S. Popovic, J.A. Flanagan, P.A. Besse, The future of magnetic sensors, *Sensors and Actuators A: Physical* 56 (1996) 39–55. [https://doi.org/10.1016/0924-4247\(96\)01285-X](https://doi.org/10.1016/0924-4247(96)01285-X).
- [10] B. Chang, S. Bai, D. Du, H. Zhang, Y. Zhou, Studies on the micro-laser spot welding of an NdFeB permanent magnet with a low carbon steel, *Journal of Materials Processing Technology* 210 (2010) 885–

891. <https://doi.org/10.1016/j.jmatprotec.2010.01.021>.

[11] S.K. Gharghan, R. Nordin, M. Ismail, Energy-efficient ZigBee-based wireless sensor network for track bicycle performance monitoring, *Sensors (Basel, Switzerland)* 14 (2014) 15573–15592.

<https://doi.org/10.3390/s140815573>.

[12] C. Schott, R. Racz, F. Betschart, R.S. Popovic, A new two-axis magnetic position sensor, in: *Proceedings of IEEE Sensors, IEEE, 12-14 June 2002*, pp. 911–915.

[13] H. Raich, P. Blümler, Design and construction of a dipolar Halbach array with a homogeneous field from identical bar magnets: NMR Mandhalas. *Concepts in Magnetic Resonance Part B: Magnetic Resonance Engineering*, 23B(1), 16-25 (2004). <https://doi.org/10.1002/CMR.B.20018>.

[14] K.S. Cho, *Viscoelasticity of Polymers: Theory and Numerical Algorithms*, 1st ed., Springer Netherlands, Dordrecht, s.l., 2016.

[15] C.-W. Feng, C.-W. Keong, Y.-P. Hsueh, Y.-Y. Wang, H.-J. Sue, Modeling of long-term creep behavior of structural epoxy adhesives, *International Journal of Adhesion and Adhesives* 25 (2005) 427–436.

<https://doi.org/10.1016/j.ijadhadh.2004.11.009>.

[16] W. Xi, W. Liu, R. Hu, Y. Yin, M. Yue, Property enhancement of bonded Nd-Fe-B magnets by composite adhesive design, *Materials & Design* 192 (2020) 108767. <https://doi.org/10.1016/j.matdes.2020.108767>.

[17] I.F. Villegas, Strength development versus process data in ultrasonic welding of thermoplastic composites with flat energy directors and its application to the definition of optimum processing parameters, *Composites Part A: Applied Science and Manufacturing* 65 (2014) 27–37.

<https://doi.org/10.1016/j.compositesa.2014.05.019>.

[18] G. Harman, J. Albers, The Ultrasonic Welding Mechanism as Applied to Aluminum-and Gold-Wire Bonding in Microelectronics, *IEEE Trans. Parts, Hybrids, Packag.* 13 (1977) 406–412.

<https://doi.org/10.1109/TPHP.1977.1135225>.

[19] F. Staab, F. Balle, Ultrasonic torsion welding of ageing-resistant Al/CFRP joints: Properties, microstructure and joint formation, *Ultrasonics* 93 (2019) 139–144.

<https://doi.org/10.1016/j.ultras.2018.11.006>.

[20] F. Balle, G. Wagner, D. Eifler, Ultrasonic Metal Welding of Aluminium Sheets to Carbon Fibre Reinforced Thermoplastic Composites, *Adv. Eng. Mater.* 11 (2009) 35–39.

<https://doi.org/10.1002/adem.200800271>.

[21] F. Balle, D. Eifler, Statistical test planning for ultrasonic welding of dissimilar materials using the example of aluminum-carbon fiber reinforced polymers (CFRP) joints, *Mat.-wiss. u. Werkstofftech* 43 (2012) 286–292. <https://doi.org/10.1002/mawe.201200943>.

- [22] F. Staab, M. Liesegang, F. Balle, Local shear strength distribution of ultrasonically welded hybrid Aluminium to CFRP joints, *Composite Structures* 248 (2020) 112481. <https://doi.org/10.1016/j.compstruct.2020.112481>.
- [23] J. Magin, F. Balle, Solid state joining of aluminum, titanium and their hybrids by ultrasonic torsion welding, *Mat.-wiss. u. Werkstofftech* 45 (2014) 1072–1083. <https://doi.org/10.1002/mawe.201400355>.
- [24] H.T. Fujii, Y. Goto, Y.S. Sato, H. Kokawa, Microstructure and lap shear strength of the weld interface in ultrasonic welding of Al alloy to stainless steel, *Scripta Materialia* 116 (2016) 135–138. <https://doi.org/10.1016/j.scriptamat.2016.02.004>.
- [25] S. Shimizu, H.T. Fujii, Y.S. Sato, H. Kokawa, M.R. Sriraman, S.S. Babu, Mechanism of weld formation during very-high-power ultrasonic additive manufacturing of Al alloy 6061, *Acta Materialia* 74 (2014) 234–243. <https://doi.org/10.1016/j.actamat.2014.04.043>.
- [26] T. Watanabe, H. Sakuyama, A. Yanagisawa, Ultrasonic welding between mild steel sheet and Al–Mg alloy sheet, *Journal of Materials Processing Technology* 209 (2009) 5475–5480. <https://doi.org/10.1016/j.jmatprotec.2009.05.006>.
- [27] V.K. Patel, S.D. Bhole, D.L. Chen, Ultrasonic spot welded AZ31 magnesium alloy: Microstructure, texture, and lap shear strength, *Materials Science and Engineering: A* 569 (2013) 78–85. <https://doi.org/10.1016/j.msea.2013.01.042>.
- [28] A. Panteli, J.D. Robson, I. Brough, P.B. Prangnell, The effect of high strain rate deformation on intermetallic reaction during ultrasonic welding aluminium to magnesium, *Materials Science and Engineering: A* 556 (2012) 31–42. <https://doi.org/10.1016/j.msea.2012.06.055>.
- [29] C. Born, H. Kuckert, G. Wagner, D. Eifler, Ultrasonic Torsion Welding of Sheet Metals to Cellular Metallic Materials, *Adv. Eng. Mater.* 5 (2003) 779–786. <https://doi.org/10.1002/adem.200310102>.
- [30] H. Kuckert, C. Born, G. Wagner, D. Eifler, Helium-tight Sealing of Glass with Metal by Ultrasonic Welding, *Adv. Eng. Mater.* 3 (2001) 903. [https://doi.org/10.1002/1527-2648\(200111\)3:11<903:AID-ADEM903>3.0.CO;2-O](https://doi.org/10.1002/1527-2648(200111)3:11<903:AID-ADEM903>3.0.CO;2-O).
- [31] B. Harras, K.C. Cole, T. Vu-Khanh, Optimization of the Ultrasonic Welding of PEEK-Carbon Composites, *Journal of Reinforced Plastics and Composites* 15 (1996) 174–182. <https://doi.org/10.1177/073168449601500203>.
- [32] U. Khan, N.Z. Khan, J. Gulati, Ultrasonic Welding of Bi-Metals: Optimizing Process Parameters for Maximum Tensile-Shear Strength and Plasticity of Welds, *Procedia Engineering* 173 (2017) 1447–1454. <https://doi.org/10.1016/j.proeng.2016.12.210>.
- [33] G. Wagner, F. Balle, D. Eifler, Ultrasonic Welding of Aluminum Alloys to Fiber Reinforced Polymers, *Adv. Eng. Mater.* 15 (2013) 792–803. <https://doi.org/10.1002/adem.201300043>.

- [34] K.F. Graff, Process Applications of Power Ultrasonics - A Review, in: 1974 Ultrasonics Symposium, IEEE, 11.11.1974 - 14.11.1974, pp. 628–641.
- [35] D. Bakavos, P.B. Prangnell, Mechanisms of joint and microstructure formation in high power ultrasonic spot welding 6111 aluminium automotive sheet, *Materials Science and Engineering: A* 527 (2010) 6320–6334. <https://doi.org/10.1016/j.msea.2010.06.038>.
- [36] M. Maeda, T. Sato, N. Inoue, D. Yagi, Y. Takahashi, Anomalous microstructure formed at the interface between copper ribbon and tin-deposited copper plate by ultrasonic bonding, *Microelectronics Reliability* 51 (2011) 130–136. <https://doi.org/10.1016/j.microrel.2010.05.009>.
- [37] M. Maeda, Y. Takahashi, M. Fukuhara, X. Wang, A. Inoue, Ultrasonic bonding of Zr55Cu30Ni5Al10 metallic glass, *Materials Science and Engineering: B* 148 (2008) 141–144. <https://doi.org/10.1016/j.mseb.2007.09.028>.
- [38] Y.-S. Choi, Y.-H. Yoo, J.-G. Kim, S.-H. Kim, A comparison of the corrosion resistance of Cu–Ni–stainless steel multilayers used for EMI shielding, *Surface and Coatings Technology* 201 (2006) 3775–3782. <https://doi.org/10.1016/j.surfcoat.2006.03.040>.
- [39] A. Ali, A. Ahmad, K.M. Deen, Multilayer ceramic coating for impeding corrosion of sintered NdFeB magnets, *Journal of Rare Earths* 27 (2009) 1003–1007. [https://doi.org/10.1016/S1002-0721\(08\)60357-9](https://doi.org/10.1016/S1002-0721(08)60357-9).
- [40] Granta Design, CES Edupack, 2018.
- [41] L. Li, A. Tirado, I.C. Nlebedim, O. Rios, B. Post, V. Kunc, R.R. Lowden, E. Lara-Curzio, R. Fredette, J. Ormerod, T.A. Lograsso, M.P. Paranthaman, Big Area Additive Manufacturing of High Performance Bonded NdFeB Magnets, *Scientific reports* 6 (2016) 36212. <https://doi.org/10.1038/srep36212>.
- [42] W. Brockmann, *Adhesive bonding: Materials, applications and technology*, Wiley-VCH, Weinheim, 2009.
- [43] S.L. Raykhere, P. Kumar, R.K. Singh, V. Parameswaran, Dynamic shear strength of adhesive joints made of metallic and composite adherents, *Materials & Design* 31 (2010) 2102–2109. <https://doi.org/10.1016/j.matdes.2009.10.043>.
- [44] M. You, Y. Zheng, X.-L. Zheng, W.-J. Liu, Effect of metal as part of fillet on the tensile shear strength of adhesively bonded single lap joints, *International Journal of Adhesion and Adhesives* 23 (2003) 365–369. [https://doi.org/10.1016/S0143-7496\(03\)00064-2](https://doi.org/10.1016/S0143-7496(03)00064-2).

Figures

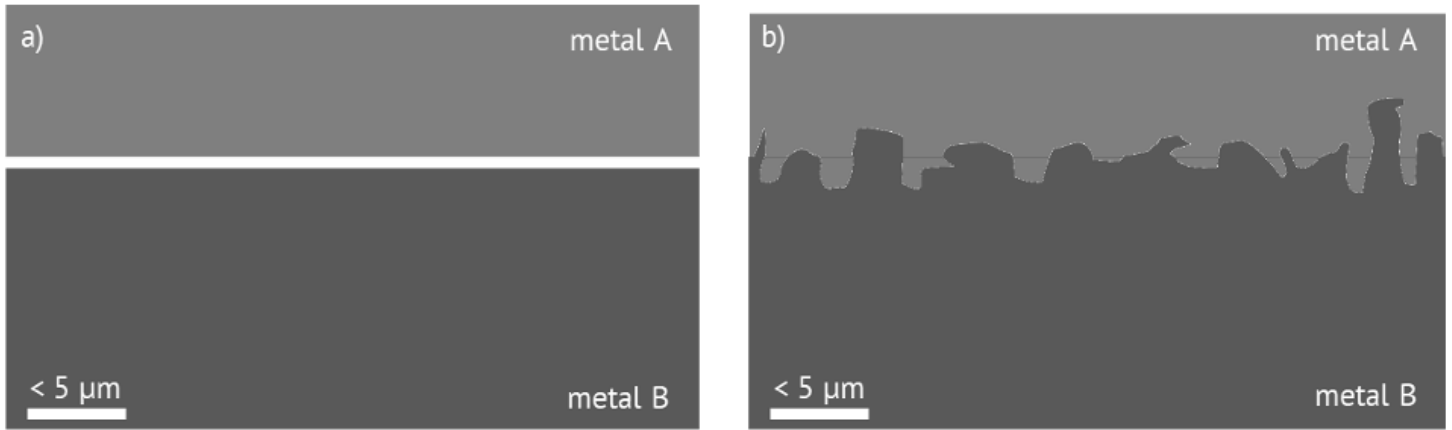


Figure 1

Mechanism of the joint formation of ultrasonic welded metal/metal joints, schematically a) initial state and b) after the welding process [23,25,34–37]

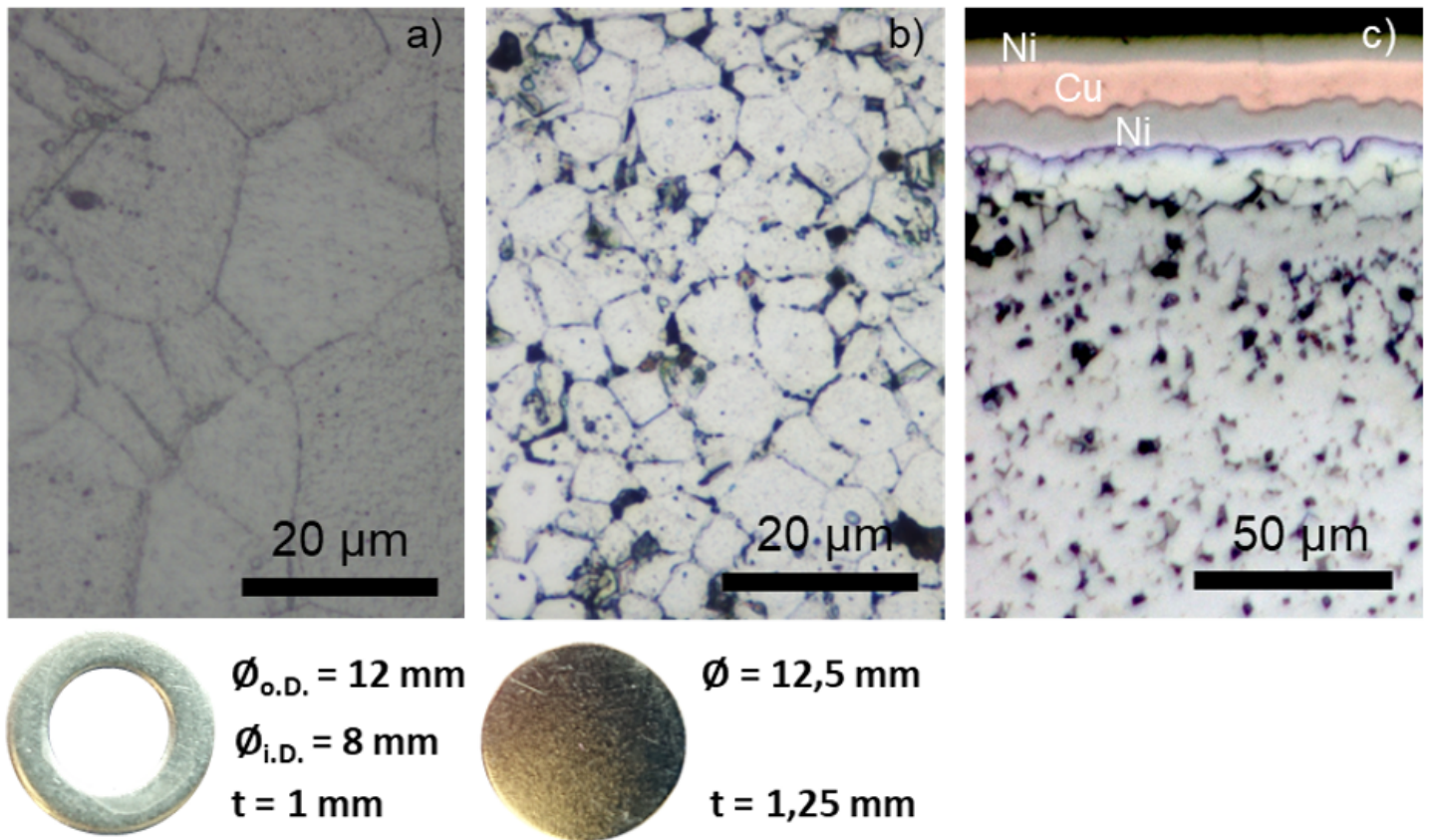


Figure 2

Microstructure of the initial joining partners a) 316L stainless steel flat ring, b) Nd2Fe14B round plate including c) a Ni/Cu/Ni coating against corrosion

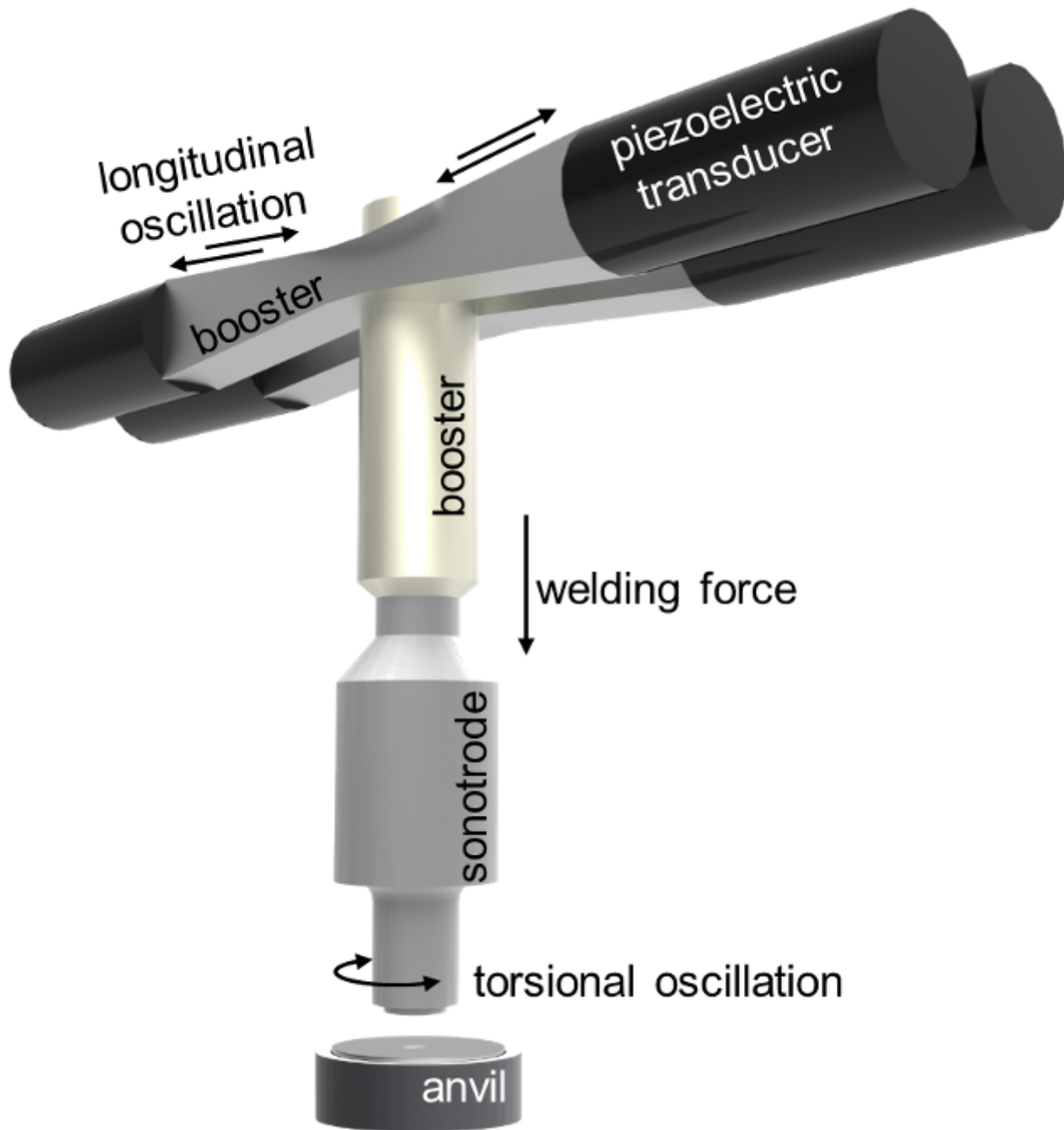


Figure 3

CAD Model of the oscillation unit and the anvil of a torsional welding machine Telsonic TSP 9000

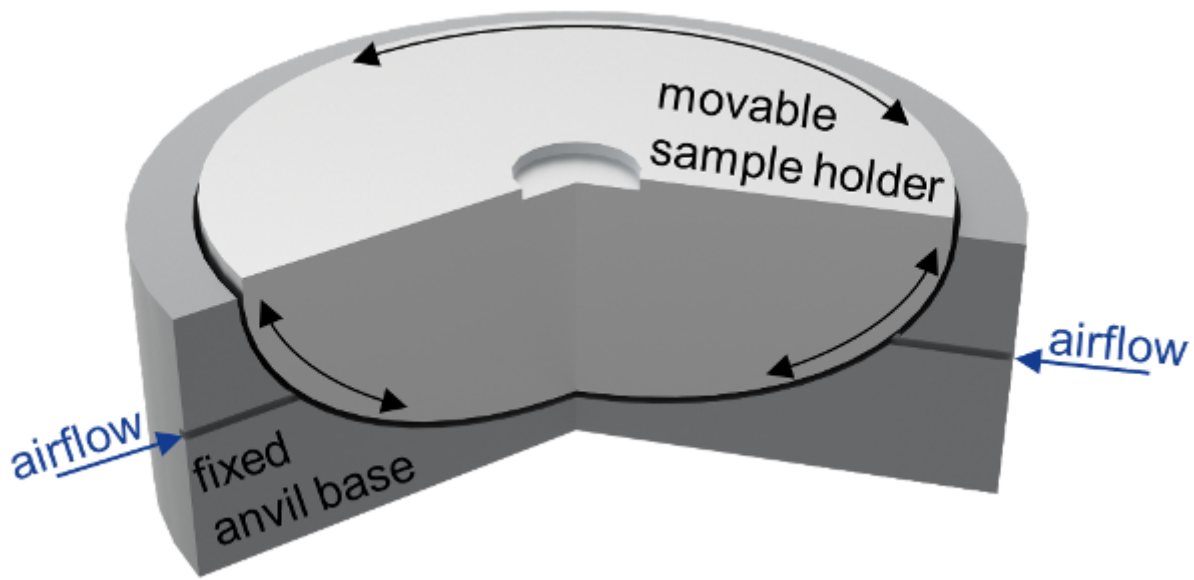


Figure 4

CAD model of the equipped air beared anvil with self-adjusting sample holder

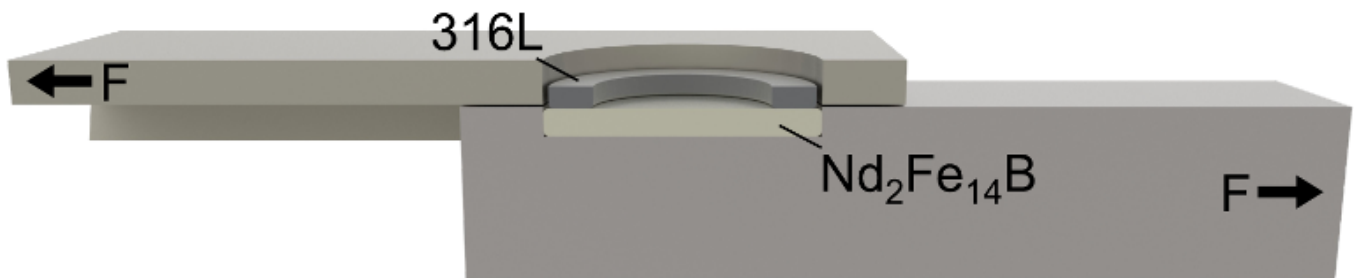


Figure 5

Insert for shear testing the ultrasonically welded joints in a tensile testing machine

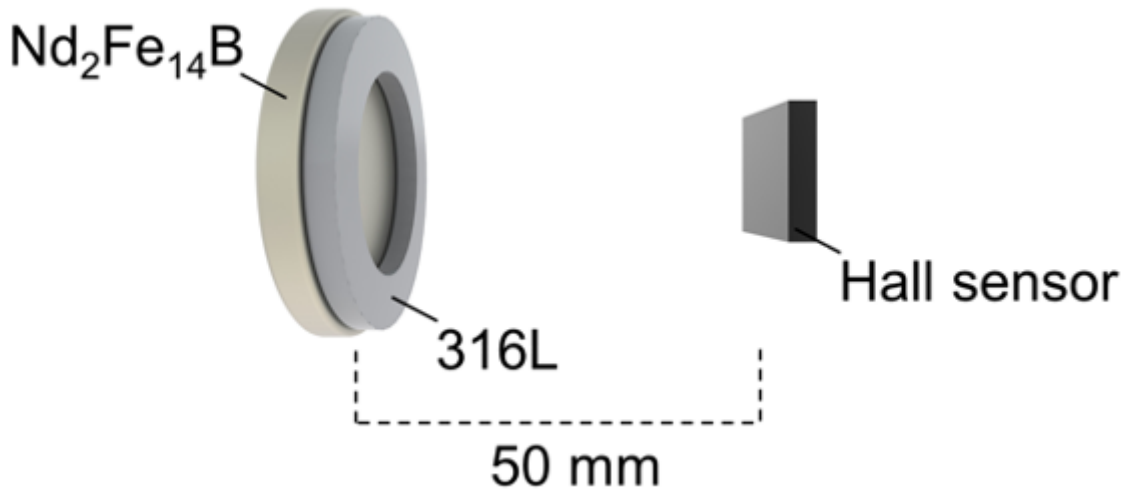


Figure 6

Open circuit magnetic flux measurement of the hybrid material systems by a hall sensor

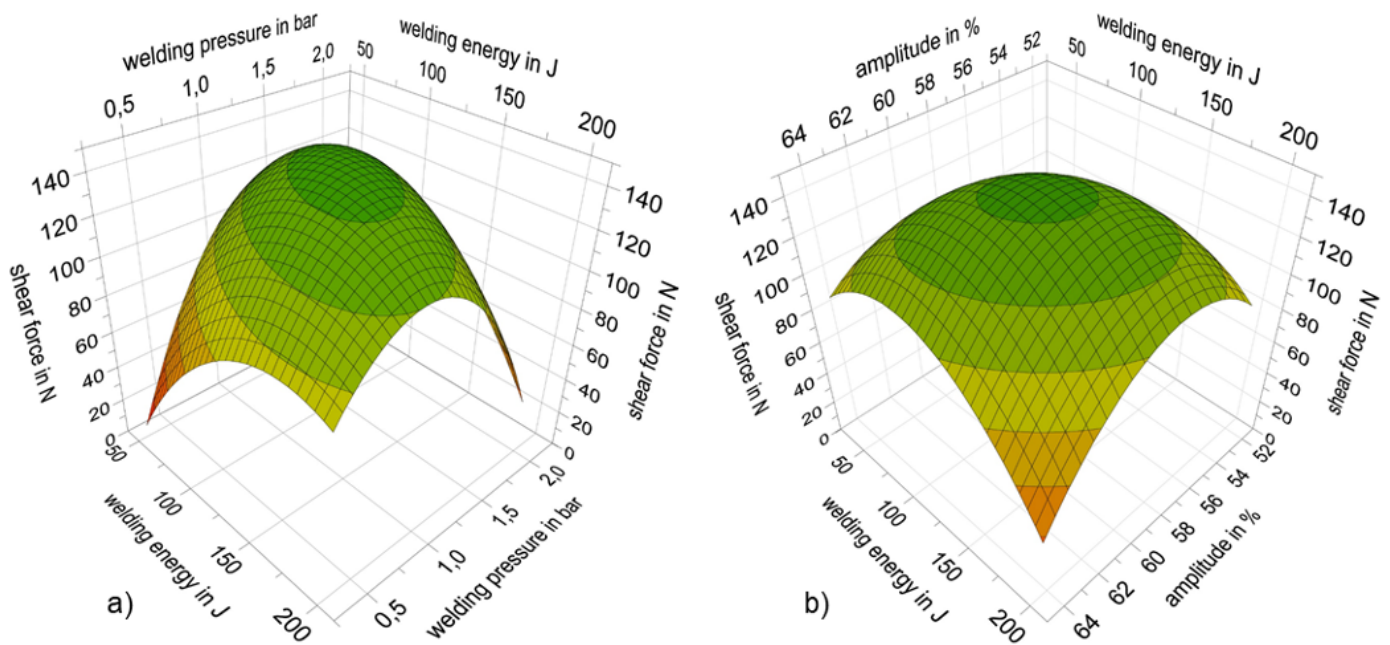


Figure 7

Maximum shear force of 316L/ $\text{Nd}_2\text{Fe}_{14}\text{B}$ joints depending on the combination of a) welding energy and pressure at an amplitude of 56%/14 μm and b) amplitude and welding energy at a welding pressure of 1.55 bar.

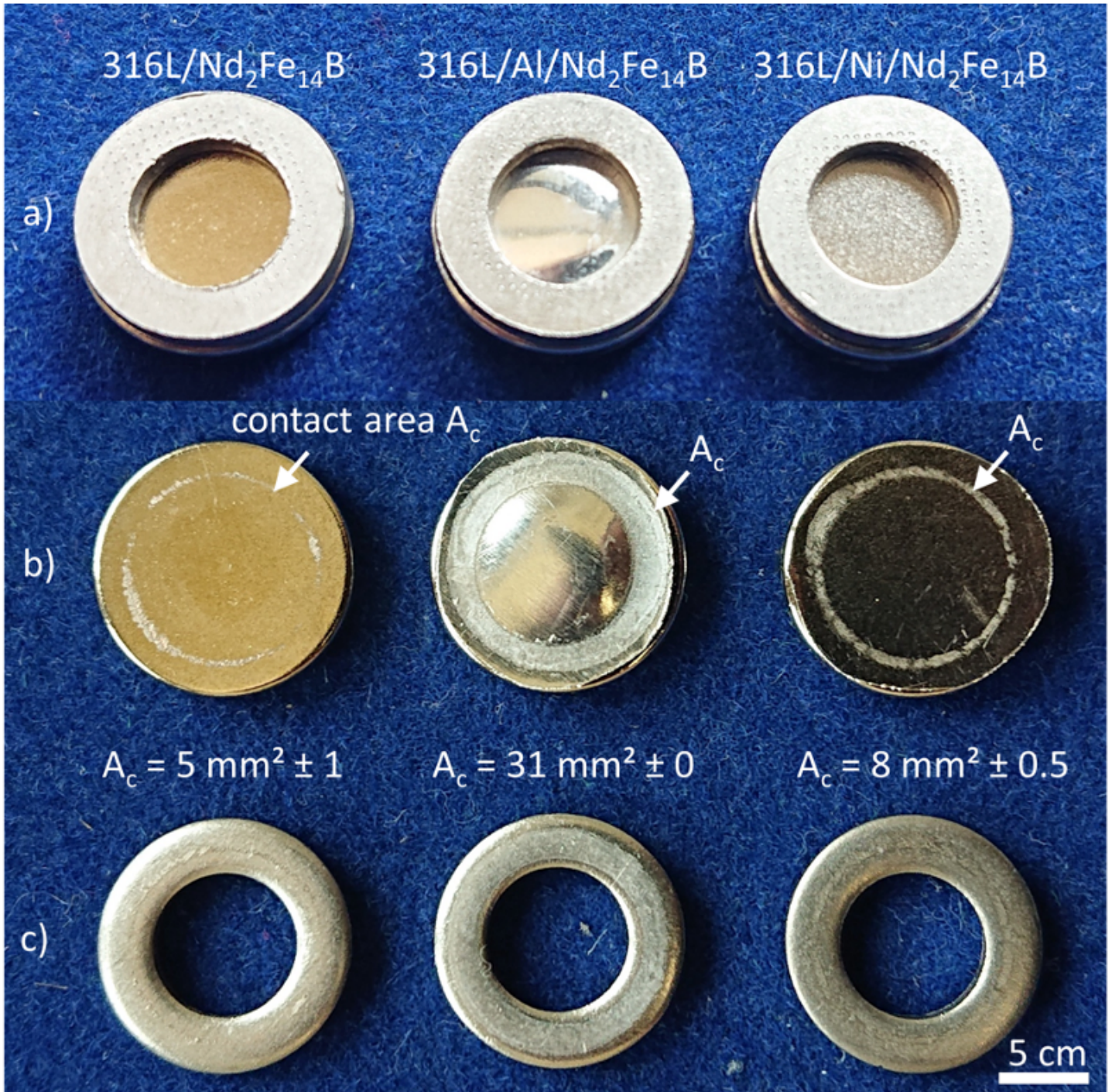


Figure 8

Ultrasonically welded joints a) different hybrid material systems and fracture surfaces of b) the lower joining partner and c) the 316L flat ring

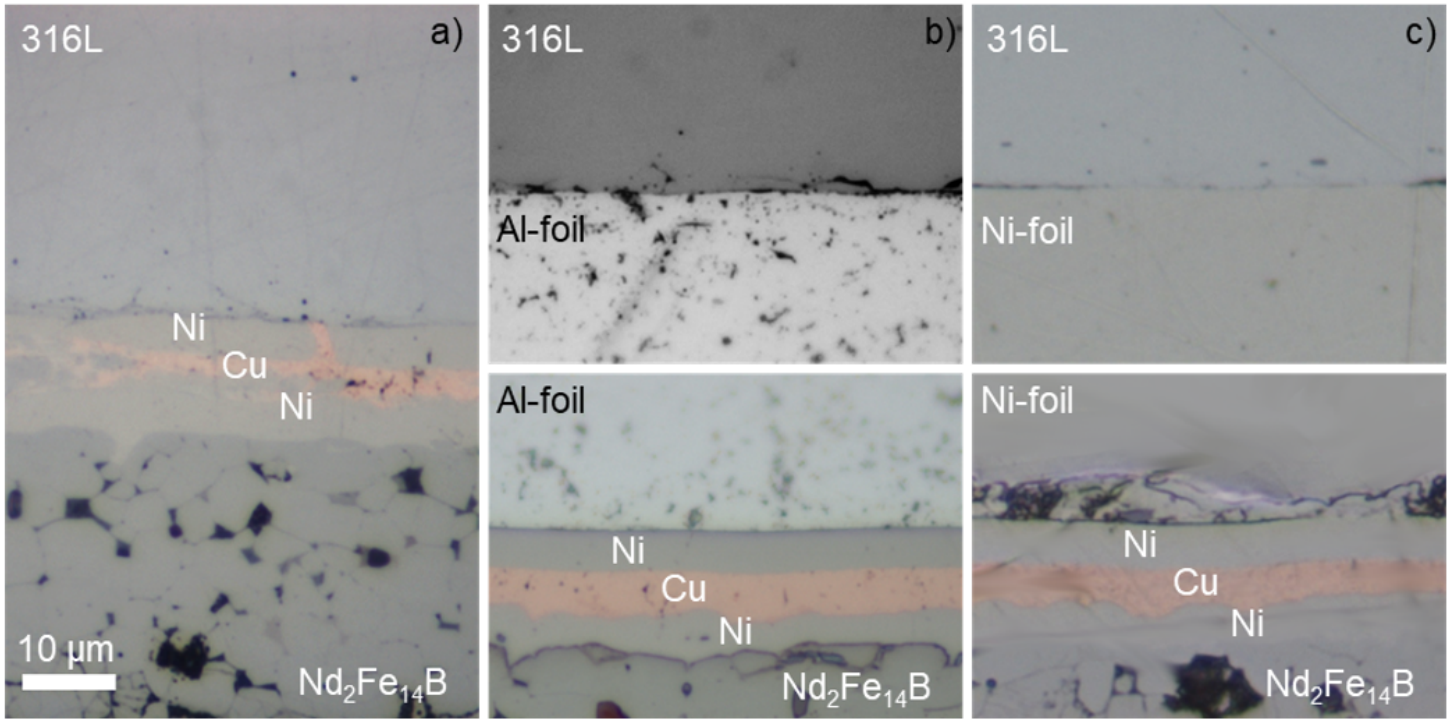


Figure 9

Microstructure of ultrasonically welded joints: a) 316L/Nd₂Fe₁₄B b) 316L/Al/Nd₂Fe₁₄B and c) 316L/Ni/Nd₂Fe₁₄B

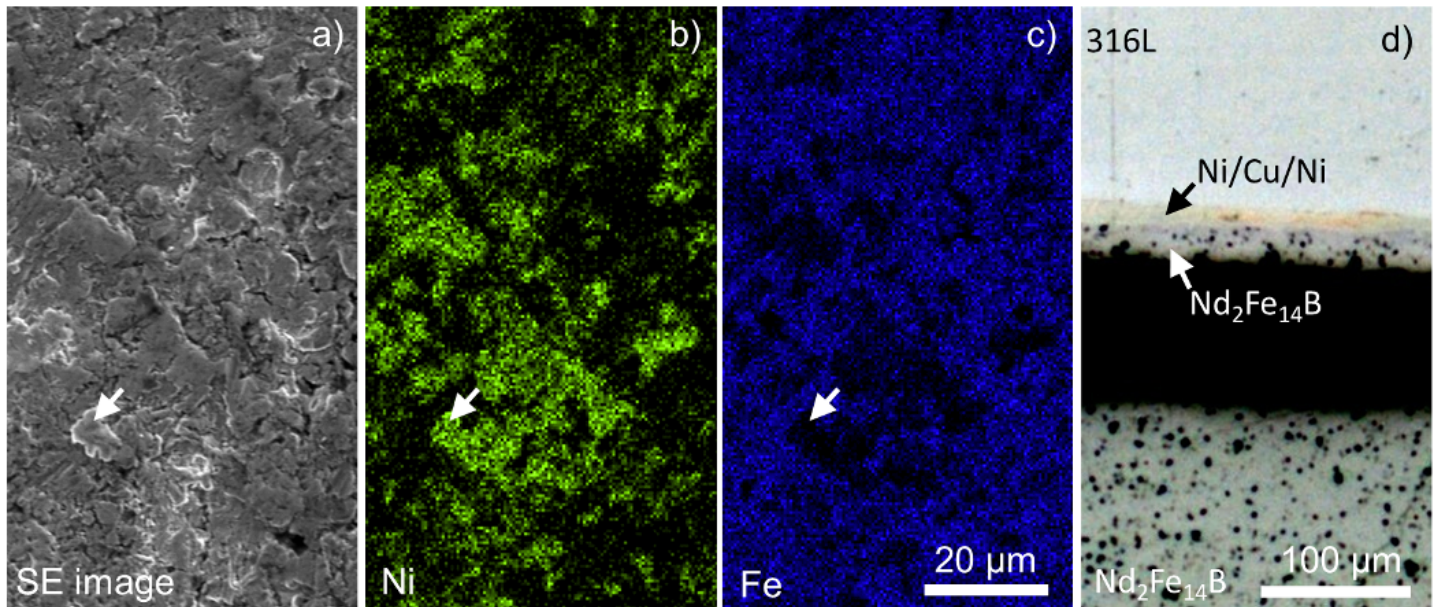


Figure 10

Scanning electron microscopy and energy dispersive X-Ray (EDX) mappings of a fracture surface of a 316L/NdFeB showing the 316L surface a) secondary electron image b) EDX mapping of Nickel c) EDX mapping of Fe and d) the microsection of a failed 316L/NdFeB joint